PTEP

Prog. Theor. Exp. Phys. **2016**, 103E01 (21 pages)
DOI: 10.1093/ptep/ptw143

Gravitational wave quasinormal mode from Population III massive black hole binaries in various models of population synthesis

Tomoya Kinugawa[1,*], Hiroyuki Nakano[2], and Takashi Nakamura[2]

[1]*Institute for Cosmic Ray Research, The University of Tokyo, Chiba 277-8582, Japan*
[2]*Department of Physics, Kyoto University, Kyoto 606-8502, Japan*
[*]E-mail: kinugawa@tap.scphys.kyoto-u.ac.jp

Received June 1, 2016; Revised August 31, 2016; Accepted September 1, 2016; Published October 21, 2016

Focusing on the remnant black holes after merging binary black holes, we show that ringdown gravitational waves of Population III binary black hole mergers can be detected at the rate of 5.9–500 events yr^{-1} $(\mathrm{SFR_p}/(10^{-2.5}\,M_\odot\,\mathrm{yr}^{-1}\,\mathrm{Mpc}^{-3}))\cdot([\mathrm{f_b}/(1+\mathrm{f_b})]/0.33)$ for various parameters and functions. This rate is estimated for events with SNR $>$ 8 for second-generation gravitational wave detectors such as KAGRA. Here, $\mathrm{SFR_p}$ and $\mathrm{f_b}$ are the peak value of the Population III star formation rate and the fraction of binaries, respectively. When we consider only events with SNR $>$ 35, the event rate becomes 0.046–4.21 events yr^{-1} $(\mathrm{SFR_p}/(10^{-2.5}\,M_\odot\,\mathrm{yr}^{-1}\,\mathrm{Mpc}^{-3}))\cdot([\mathrm{f_b}/(1+\mathrm{f_b})]/0.33)$. This suggest that for a remnant black hole spin of $q_f > 0.95$ we have an event rate of quasinormal modes with SNR $>$ 35 of less than 0.037 events yr^{-1} $(\mathrm{SFR_p}/(10^{-2.5}\,M_\odot\,\mathrm{yr}^{-1}\,\mathrm{Mpc}^{-3}))\cdot([\mathrm{f_b}/(1+\mathrm{f_b})]/0.33)$, while it is 3–30 events yr^{-1} $(\mathrm{SFR_p}/(10^{-2.5}\,M_\odot\,\mathrm{yr}^{-1}\,\mathrm{Mpc}^{-3}))\cdot([\mathrm{f_b}/(1+\mathrm{f_b})]/0.33)$ for third-generation detectors such as the Einstein Telescope. If we detect many Population III binary black hole mergers, it may be possible to constrain the Population III binary evolution paths not only by the mass distribution but also by the spin distribution.

Subject Index E01, E02, E31, E38

1. Introduction

The final part of gravitational waves (GWs) from merging binary black holes (BBHs) is called the ringdown phase. When the remnant compact object is a black hole (BH), this phase is described by quasinormal modes (QNMs) of the BH (see, e.g., Ref. [1]). In general, the BH is expected as the Kerr spacetime [2],

$$ds^2 = -\left(1-\frac{2Mr}{\Sigma}\right)dt^2 - \frac{4Mar\sin^2\theta}{\Sigma}dtd\phi + \frac{\Sigma}{\Delta}dr^2 + \Sigma d\theta^2 + \left(r^2+a^2+\frac{2Ma^2r}{\Sigma}\sin^2\theta\right)\sin^2\theta d\phi^2, \quad (1)$$

where $\Delta = r^2 - 2Mr + a^2$ and $\Sigma = r^2 + a^2\cos^2\theta$, with mass M and spin a. In Eq. (1), we used the units of $c = G = 1$. The detection of QNM GWs not only gives a precise estimation of the BH's mass and spin, but also tests Einstein's general relativity (see the extensive review in [3]).

In our previous paper [4], using the recent population synthesis results of Population III (Pop III) massive BBHs [5,6], we discussed the event rate of QNM GWs by second-generation gravitational

wave detectors such as Advanced LIGO [7], Advanced Virgo [8], and KAGRA [9,10]. Since there are various parameters and functions in the population synthesis calculation, we extensively examine BBH binary formations in this paper. Then, we calculate the remnant BH's mass M_f and the non-dimensional spin $q_f = a_f/M_f$ via fitting formulas [11], and the event rate for each model.

This paper is organized as follows. In Sect. 2, we summarize our Pop III binary population synthesis calculation, and prepare ten models. In Sect. 3, we show the mass ratio distributions of BBH remnants for each model. The dependences on initial distribution functions, binary parameters, etc. are also discussed. In Sect. 4, we obtain the spin distributions of BBH remnants for various parameters. Using the results presented in the above sections, we calculate the mass and spin distributions of the remnant BHs after merger in Sect. 5, and show the event rates of QNMs for each model in KAGRA. Section 6 is devoted to discussions.

2. Population III binary population synthesis calculation

To estimate the detection rate of GWs from Pop III BBH mergers, it is necessary to know how many Pop III binaries become BBHs which merge within the Hubble time. Here, we use the binary population synthesis method of Monte Carlo simulation of binary evolutions. The Pop III binary population synthesis code [4–6] has been upgraded from the binary population synthesis code [12][1] for Pop III binaries. In this paper, we calculate the same models as Ref. [6] using the same methods as Ref. [6] in order to obtain the mass ratio distribution and the spin distribution. In this section, we review the calculation method and models. Note that in this paper, we do not consider the kick models and the worst model discussed in Ref. [6] for simplicity, because in these models, BBHs have misaligned spins and the final spins after merger are too complex.

First, we need to give the initial conditions when a binary is born. The initial conditions such as primary mass M_1, mass ratio M_2/M_1 (where M_2 is the secondary mass), separation a, and orbital eccentricity e are decided by the Monte Carlo method with initial distribution functions such as the initial mass function (IMF), the initial mass ratio function (IMRF), the initial separation function (ISF), and the initial eccentricity function (IEF). For example, in our standard model, we use a flat IMF, a flat IMRF, a logflat ISF, and an IEF with a function $\propto e$. There are no observations of Pop III binaries because they were born at the early universe. Thus, we do not know the initial distribution functions of Pop III binaries from observations. For the IMF, however, the recent simulations [13,14] may suggest a flat IMF, and therefore we adapt the flat IMF. For the other initial distribution functions, we adapt those of the Pop I case, where a Pop I star is a solar-like star. The above set of initial distribution functions is called our standard model of 140 cases with the optimistic core-merger criterion in this paper.

Second, we calculate the evolution of each star, and if the star satisfies a condition of binary interactions, we evaluate the effects of binary interactions and change M_1, M_2, a, and e. As the binary interactions, we treat the Roche lobe overflow (RLOF), the common envelope (CE) phase, the tidal effect, the supernova effect, and the gravitational radiation. The RLOF is stable mass transfer, while unstable mass transfer becomes the CE phase when the donor star is a giant. Here, we need some parameters for the calculation of the RLOF and CE phases.

In the case of the RLOF, we use the loss fraction β of transfered stellar matter defined as

$$\dot{M}_2 = -(1-\beta)\dot{M}_1, \tag{2}$$

[1] http://astronomy.swin.edu.au/∼jhurley/.

where $\dot{M}_2$ is the mass accretion rate of the receiver star and $\dot{M}_1$ is the mass loss rate of the donor star. In our standard model, β is determined by Hurley's function [12], which has been discussed for the Pop I case. When the receiver star is in the main sequence phase or in the He-burning phase, we assume that the accretion rate is described by

$$\dot{M}_2 = -\min\left(10\frac{\tau_{\dot{M}}}{\tau_{\rm KH,2}}, 1\right)\dot{M}_1, \tag{3}$$

where $\tau_{\dot{M}}$ is the accretion time scale defined by

$$\tau_{\dot{M}} \equiv \frac{M_2}{\dot{M}_1}, \tag{4}$$

and the Kelvin–Helmholtz timescale $\tau_{\rm KH,2}$ is defined by

$$\tau_{\rm KH,2} = \frac{GM_2(M_2 - M_{\rm c,2})}{L_2 R_2}. \tag{5}$$

Here, M_2, $M_{\rm c,2}$, L_2, and R_2 are the mass, the core mass, the luminosity, and the radius of the receiver star, respectively. When the receiver star is in the He-shell burning phase, we assume that the receiver star can get all the transfered matter from the donor star, i.e.,

$$\dot{M}_2 = -\dot{M}_1. \tag{6}$$

Although we use the β function defined by Hurley et al. [12] in our standard model, we also treat the accretion rate of the receiver star described by the constant β parameter. This is because the accretion rate of a receiver star which is not a compact object is not understood well. Furthermore, in our previous study [6], we have shown that the Hurley fitting formula is consistent with $\beta = 0$ in the Pop III binary case. Thus, we also discuss the cases of $\beta = 0.5$ and $\beta = 1$. It is noted that the stability of the mass transfer changes if the mass transfer is non-conservative ($\beta > 0$). We use the criterion given in Ref. [15] as

$$\begin{aligned}\zeta_{\rm L} &= \frac{d\log R_{\rm L,1}}{d\log M_1} \\ &= \left[\left(0.33 + 0.13\frac{M_1}{M_2}\right)\left(1 + \frac{M_1}{M_2} - \beta\frac{M_1}{M_2}\right) + (1-\beta)\left(\left(\frac{M_1}{M_2}\right)^2 - 1\right) - \beta\frac{M_1}{M_2}\right] \Big/ \left(1 + \frac{M_1}{M_2}\right),\end{aligned} \tag{7}$$

where M_1 and $R_{\rm L,1}$ are the mass and the Roche lobe radius of the donor star. If $\zeta_{\rm ad} = d\log R_{\rm ad,1}/d\log M_1 < \zeta_{\rm L}$, where $R_{\rm ad,1}$ is the radius of the donor star, in the hydrostatic equilibrium of the donor star, the binary starts a dynamically unstable mass transfer such as the CE phase. When the receiver star is a compact object such as a neutron star or a BH, we always use $\beta = 0$ and the upper limit of the accretion rate is limited by the Eddington accretion rate defined by

$$\begin{aligned}\dot{M}_{\rm Edd} &= \frac{4\pi c R_2}{\kappa_{\rm T}} \\ &= 2.08\times10^{-3}\,(1+X)^{-1}\left(\frac{R_2}{R_\odot}\right) M_\odot\,{\rm yr}^{-1},\end{aligned} \tag{8}$$

Table 1. The model parameters in this paper. Each column represents the model name, the initial mass function (IMF), the initial eccentricity function (IEF), the common envelope (CE) parameter $\alpha\lambda$, and the loss fraction β of the transfer of stellar matter at the Roche lobe overflow (RLOF) in each model.

Model	IMF	IEF	$\alpha\lambda$	β
our standard	flat	e	1	function
IMF: logflat	M^{-1}	e	1	function
IMF: Salpeter	Salpeter	e	1	function
IEF: const.	flat	const.	1	function
IEF: $e^{-0.5}$	flat	$e^{-0.5}$	1	function
$\alpha\lambda = 0.01$	flat	e	0.01	function
$\alpha\lambda = 0.1$	flat	e	0.1	function
$\alpha\lambda = 10$	flat	e	10	function
$\beta = 0.5$	flat	e	1	0.5
$\beta = 1$	flat	e	1	1

where $\kappa_{\rm T} = 0.2\,(1+X)\,{\rm cm}^2\,{\rm g}^{-1}$ is the Thomson scattering opacity and $X(=0.76)$ is the H-mass fraction for Pop III stars.

At the CE phase, the companion star plunges into the envelope of the donor star and spirals in. The orbital separation after the CE phase $a_{\rm f}$ is calculated by the energy formalism [16] described by

$$\alpha\left(\frac{GM_{\rm c,1}M_2}{2a_{\rm f}}-\frac{GM_1M_2}{2a_{\rm i}}\right)=\frac{GM_1M_{\rm env,1}}{\lambda R_1}, \tag{9}$$

where $a_{\rm i}$, α, and λ are the orbital separation before the CE phase, the efficiency, and the binding energy parameter, respectively. In our standard model, we adopt $\alpha\lambda = 1$. We also calculate the $\alpha\lambda = 0.01$, 0.1. and 10 cases in this paper.

Finally, if a binary becomes a BBH, we calculate the merger time from the gravitational radiation reaction, and check whether the BBH can merge within the Hubble time or not. We repeat these calculations and take the statistics of BBH mergers.

To study the dependence of Pop III BBH properties on the initial distribution functions and binary parameters, we calculate ten models with the Pop III binary population synthesis method [5,6] in this paper. Table 1 shows the initial distribution functions and the binary parameters of each model. The columns show the model name, IMF, IEF, the CE parameter $\alpha\lambda$, and the loss fraction β of transfered stellar matter at the RLOF in each model.

3. The mass ratio distributions of binary black hole remnants

Figures 1–5 show the initial mass ratio distributions and the mass ratio distributions of merging BBHs. The RLOF tends to make binaries of equal mass. Thus, the BBH mass ratio distributions depend on how many binaries evolve via the RLOF. Population III stars with mass $< 50\,M_\odot$ evolve as blue giants [5,17]. Thus, in the case of the IMF that light stars are in the majority, the binaries tend to evolve only via the RLOF, not via the CE phase. Therefore, the steeper IMFs tend to derive many equal-mass BBHs. In this calculation, since we adopt the minimum mass ratio as $10M_\odot/M_1$, the initial mass ratio distribution of models with the IMF that light stars are the majority is up to $M_2/M_1 = 1$ *ab initio* (see Figs. 1 and 2).

On the other hand, if we change the IEF, the mass ratio distribution does not change much. Thus, the dependence on the IEF is not so large (see Figs. 1 and 3).

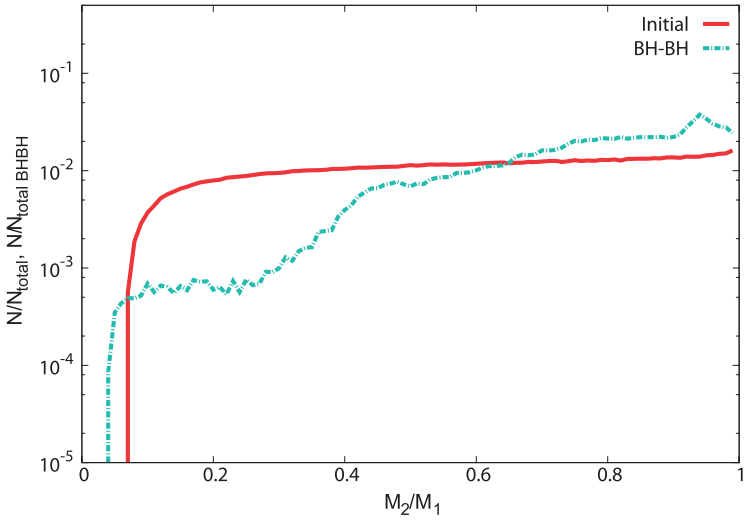

Fig. 1. The distribution of mass ratio $M_2/M_1 \leq 1$ for our standard model. The distributions of the initial mass ratio and the one when the binaries become BBHs which merge within the Hubble time are shown as red and light blue lines, respectively. The initial mass ratio distribution is normalized by the total binary number $N_{\rm total} = 10^6$, while the one when the binaries become merging BBHs is normalized by the total merging binary number $N_{\rm total\,BHBH} = 128897$.

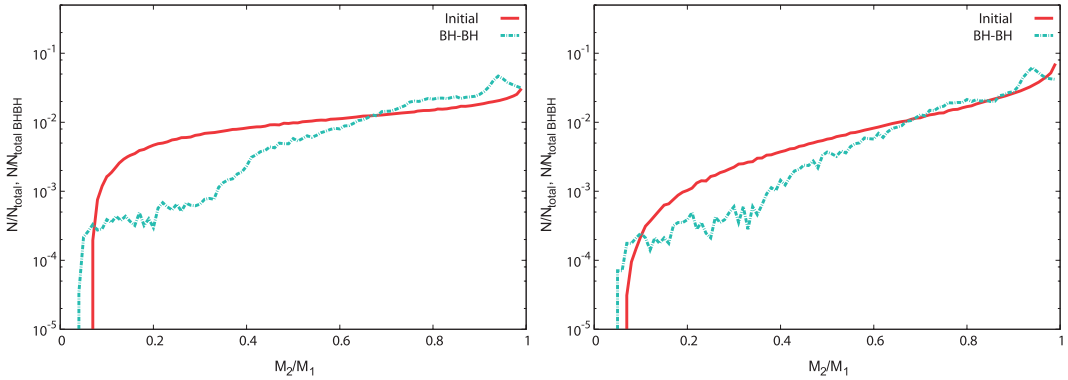

Fig. 2. The distributions of mass ratio $M_2/M_1 \leq 1$ for the IMF: logflat model (left) and IMF: Salpeter model (right). The format is the same as Fig. 1.

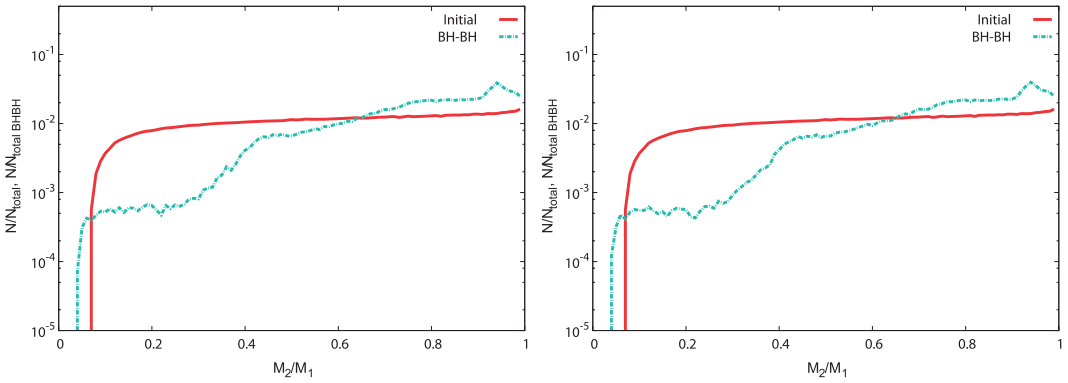

Fig. 3. The distributions of mass ratio $M_2/M_1 \leq 1$ for the IEF: $e = $ const. (left) and IEF: $e^{-0.5}$ models (right). The format is the same as Fig. 1.

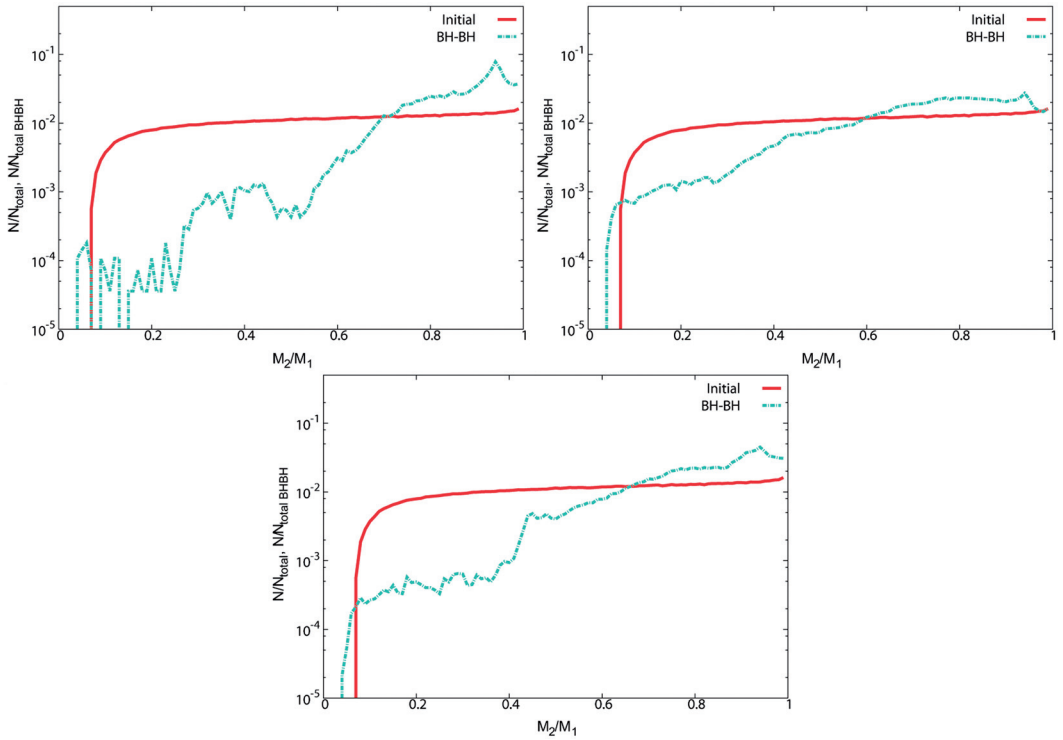

Fig. 4. The distributions of mass ratio $M_2/M_1 \leq 1$ for the $\alpha\lambda = 0.01$ (top left), $\alpha\lambda = 0.1$ (top right), and $\alpha\lambda = 10$ (bottom) models. The format is the same as Fig. 1.

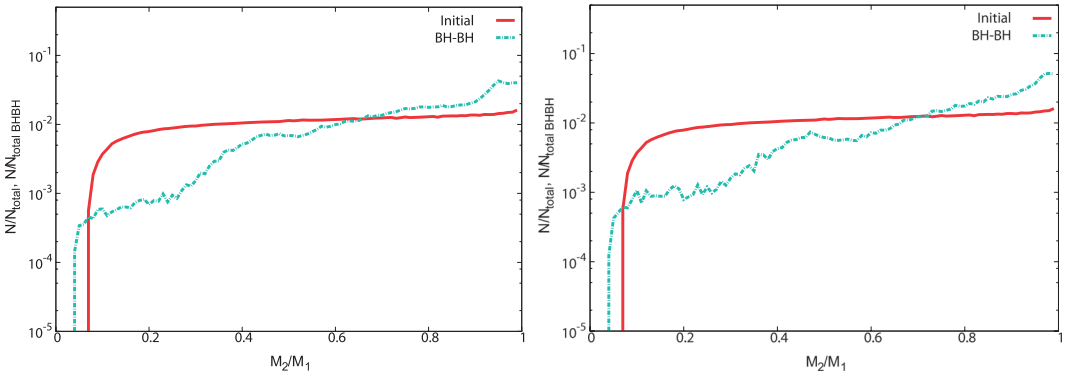

Fig. 5. The distributions of mass ratio $M_2/M_1 \leq 1$ for the $\beta = 0.5$ (left) and $\beta = 1$ models (right). The format is the same as Fig. 1.

For the CE parameter dependence (see Figs. 1 and 4), small mass ratio binaries in the model of $\alpha\lambda = 0.001$ are much fewer than those in the other models. In the $\alpha\lambda = 0.001$ model, all the binaries which evolve via the CE phase merge during the CE phase due to too-small $\alpha\lambda$. Thus, the merging BBHs in this model evolve only via the RLOF, and become of equal mass by the RLOF. The change is not large between the models with CE parameters $\alpha\lambda = 0.1$ and 10.

As for the mass loss fraction β (see Figs. 1 and 5), when β becomes large, there are three effects. First, binaries tend not to enter the CE phase. Second, the mass accretion by RLOF becomes not to be effective. Third, RLOF tends to finish early. The first effect makes binaries evolve via RLOF. However, the second and third effects have a negative impact on the tendency to become equal mass. Thus, the mass ratio distributions of the $\beta = 0.5$ and 1 models look similar to our standard model.

4. The spin distributions of binary black hole remnants

We calculate the spin evolution of binaries using the tidal friction. We use the initial spin distribution and the tidal friction calculations as in Refs. [5,12]. When the Pop III star becomes a BH, we calculate the BH's spin using the total angular momentum of the progenitor. If the estimated spin of the BH is more than the Thorne limit $q_{\rm Thorne} = 0.998$ [18], we assign the non-dimensional spin parameter $q = q_{\rm Thorne}$.

We ignore the spin up by the accretion during a mass transfer after the star became a BH for the following reason. The spin up by the accretion is calculated as

$$\begin{aligned} \delta q =& \frac{\delta J}{G M_{\rm BH}^2/c} \\ =& \sqrt{12}\frac{\delta M}{M_{\rm BH}}, \end{aligned} \tag{10}$$

where δJ, $M_{\rm BH}$, δM are the gain in angular momentum, the BH's mass, and the gain of the BH's mass, respectively. Since the accretion rate of the BH during RLOF is the Eddington rate, the gain of the BH's mass is

$$\delta M \sim \dot{M}_{\rm Edd}\, t_{\rm life}, \tag{11}$$

where $t_{\rm life}$ is the lifetime of the Pop III star. The Eddington accretion rate is given by

$$\dot{M}_{\rm Edd} \sim 10^{-7} \left(\frac{M_{\rm BH}}{30\,M_\odot}\right) M_\odot\,{\rm yr}^{-1}, \tag{12}$$

and the lifetime of the massive star is $t_{\rm life} \sim 1\,{\rm Myr}$. As a result, we have $\delta q \sim 0.01$, and the spin up by the accretion during RLOF is negligible. On the other hand, the accretion rate during the CE phase is $\dot{M} \sim 10^{-3}\,M_\odot\,{\rm yr}^{-1}$ [19], and the timescale of the CE phase is about the thermal timescale of a red giant $t_{\rm KH} \sim 10^2\,{\rm yr}$ or less. As a result, we have $\delta q \leq 0.1$, and the spin up by the accretion during the CE phase is negligible, too.

Figures 6–15 show the spin distributions of merging BBHs and cross-section views of these spin distributions. The spins of merging Pop III BBH can be roughly classified into three types: group 1, in which both BHs have high spins $q \sim 0.998$; group 2, in which both BHs have low spins; and group 3, in which one of the pair has high spin $q \sim 0.998$ and the other has low spin.

When the BH progenitor evolves via the CE phase, the Pop III BH has low spin, and vice versa. If a Pop III star which is a giant evolves via the CE phase, the Pop III star loses the envelope and almost all the angular momentum due to the envelope evaporation. On the other hand, if the Pop III star evolves without the CE phase, the Pop III star can have a high angular momentum. Therefore, group 1 progenitors evolve without the CE phase and the envelopes of the progenitors remain. In group 2, both stars evolve via the CE phase and they lose their envelopes and almost all their angular momentum. In group 3, the primary evolves via the CE phase and the secondary evolves without the CE phase, or vice versa.

The IMF dependence of merging Pop III BBH spins is described as follows (see Figs. 6, 7, and 8). Population III stars with masses $< 50\,M_\odot$ evolve as a blue giant. Thus, in the case of an IMF that light stars are in the majority, such as the Salpeter IMF, the binaries tend to evolve only via RLOF, not via the CE phase. Therefore, for a steeper IMF, we have larger numbers of merging Pop III BBHs

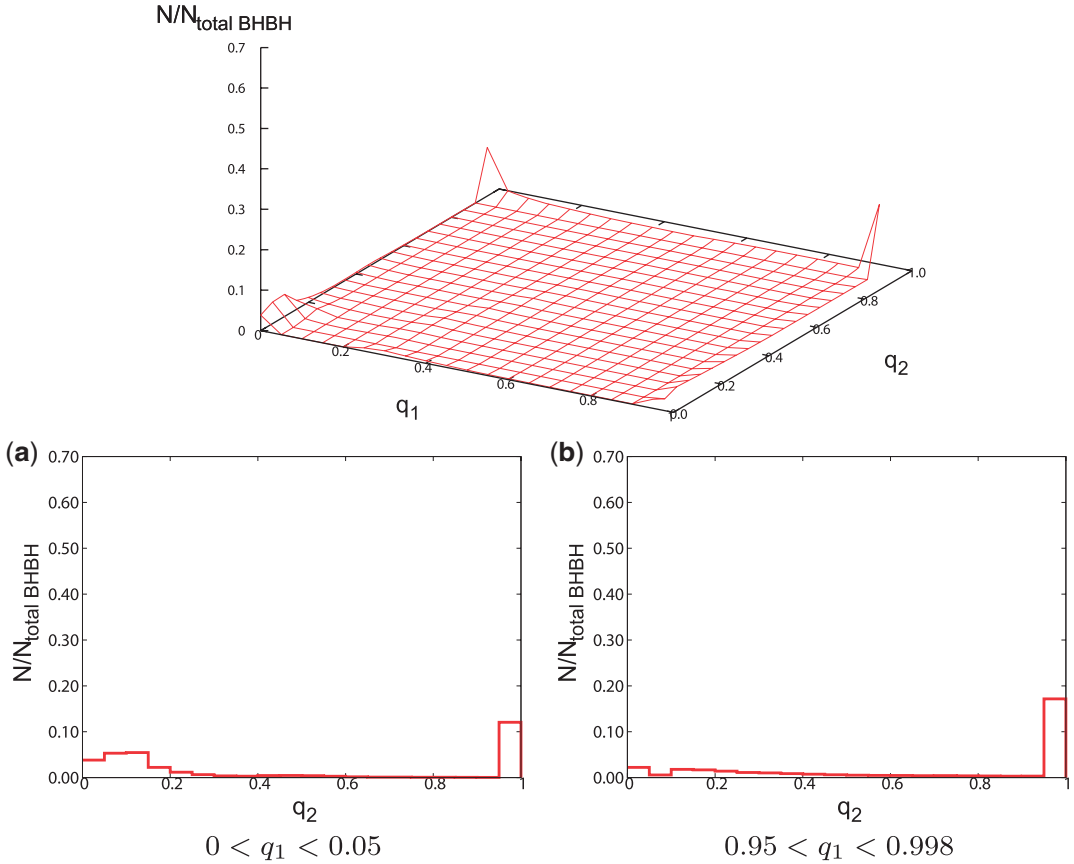

Fig. 6. (Top) The distribution of spin parameters for our standard model when each star becomes a BH. q_1 and q_2 are the spin parameters of the primary and the secondary BHs, respectively. The distribution when the binaries become merging BBHs is normalized by the total merging BBH number $N_{\rm total\,BHBH} = 128897$, with the grid separation being $\Delta q_1 = \Delta q_2 = 0.05$. (Bottom) Cross-section views of the distribution of spin parameters for our standard model. (a) The distribution of q_2 for $0 < q_1 < 0.05$. We can see that the q_2 distribution has bimodal peaks at $0 < q_2 < 0.15$ and $0.95 < q_2 < 0.998$. (b) The distribution of q_2 for $0.95 < q_1 < 0.998$. We see that the large value of q_2 is the majority, so that there is a group in which both q_1 and q_2 are large.

which have high spins. In particular, in the case of the Salpeter IMF about 40% of the BBHs have spins $q_1 > 0.95$ and $q_2 > 0.95$.

As for the IEF dependence, there is no tendency like the mass ratio distribution (see Figs. 6, 9, and 10).

The dependence on the CE parameter can be considered as follows (see Figs. 6, 11, 12, and 13). In the $\alpha\lambda = 0.01$ model, almost all merging Pop III BBHs have high spins. About 60% of merging Pop III BBHs have $q_1 > 0.95$ and $q_2 > 0.95$ (i.e., group 1). The reason for this is that the progenitors which evolve via the CE phase always merge during the CE phase due to too-small $\alpha\lambda$. Thus, the progenitors of merging Pop III BBHs in this model evolve only via RLOF and they do not lose angular momentum via the CE phase. In the case of the $\alpha\lambda = 0.1$ model, the fraction of group 2 is lower than that of our standard model, like the $\alpha\lambda = 0.01$ model. However, the fraction of group 1 is almost the same as that of our standard model, and the fraction of group 3 is larger than that of our standard model, unlike the $\alpha\lambda = 0.01$ model. The reason for this is that although progenitors which enter CE phases twice merge during the CE phase due to small $\alpha\lambda$, progenitors which enter

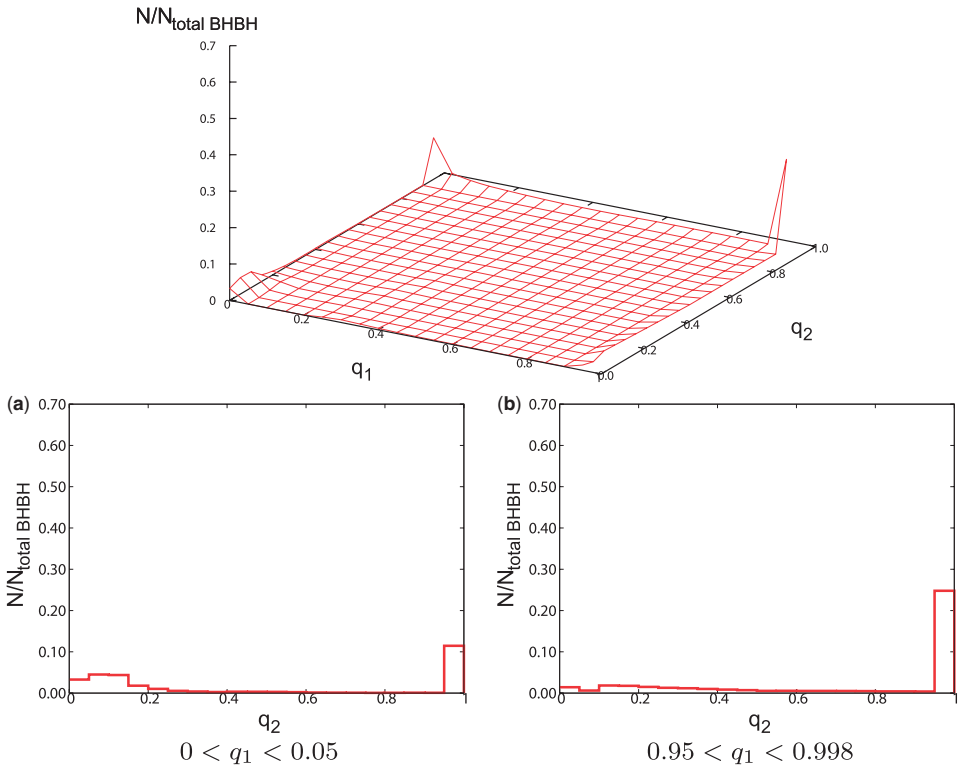

Fig. 7. (Top) The distribution of spin parameters for the IMF: logflat model, with $N_{\rm total\,BHBH} = 87596$. (Bottom) Cross-section views of the distribution of spin parameters for the IMF: logflat model. The format is the same as Fig. 6.

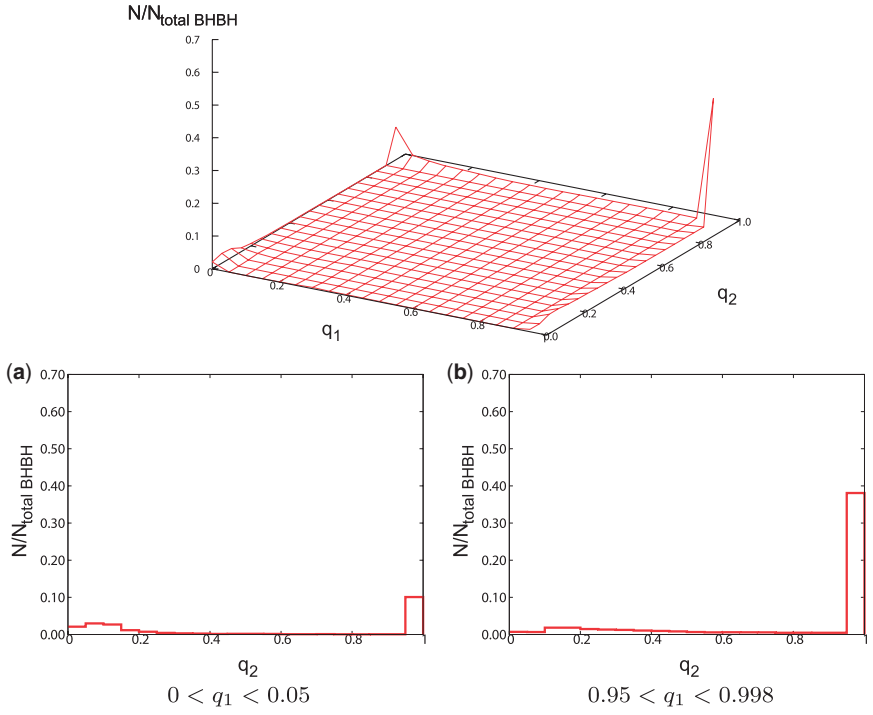

Fig. 8. (Top) The distribution of spin parameters for the IMF: Salpeter model, with $N_{\rm total\,BHBH} = 28376$. (Bottom) Cross-section views of the distribution of spin parameters for the IMF: Salpeter model. The format is the same as Fig. 6.

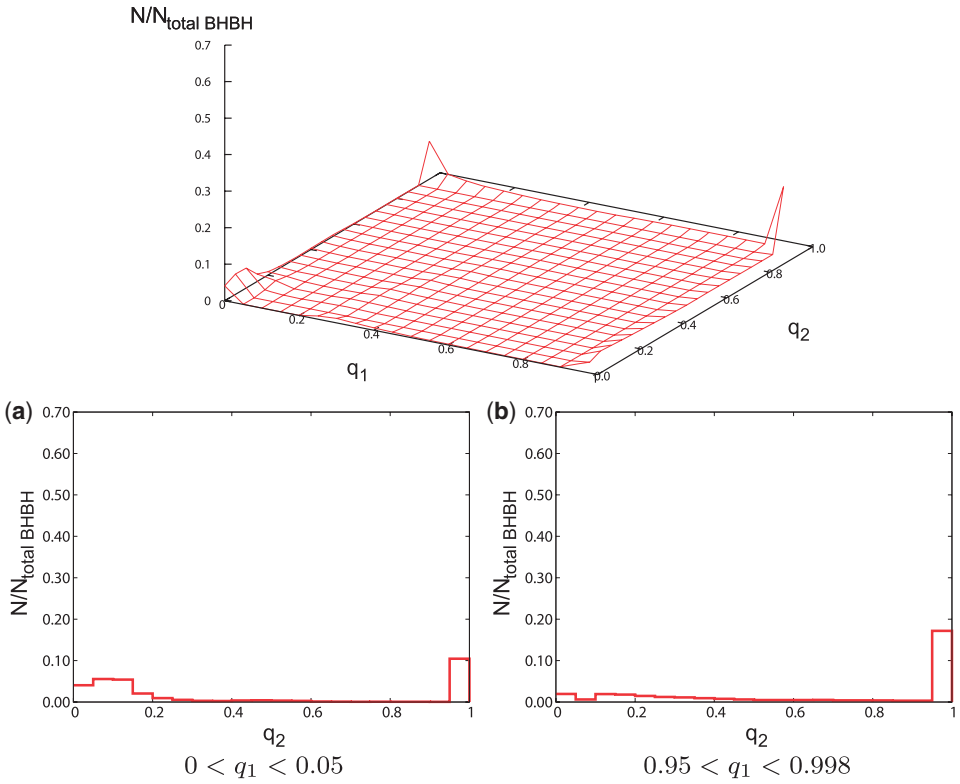

Fig. 9. (Top) The distribution of spin parameters for the IEF: e = const. model, with $N_{\rm total\,BHBH} = 124711$. (Bottom) Cross-section views of the distribution of spin parameters for the IEF: e = const. model. The format is the same as Fig. 6.

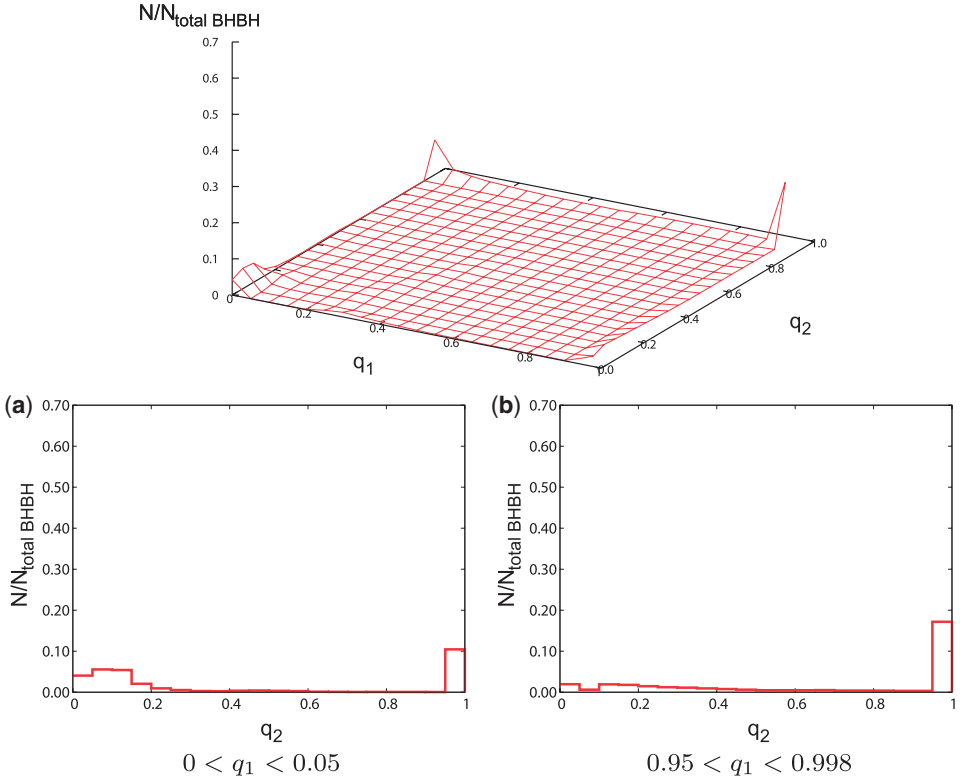

Fig. 10. (Top) The distribution of spin parameters for the IEF: $e^{-0.5}$ model, with $N_{\rm total\,BHBH} = 121495$. (Bottom) Cross-section views of the distribution of spin parameters for the IEF: $e^{-0.5}$ model. The format is the same as Fig. 6.

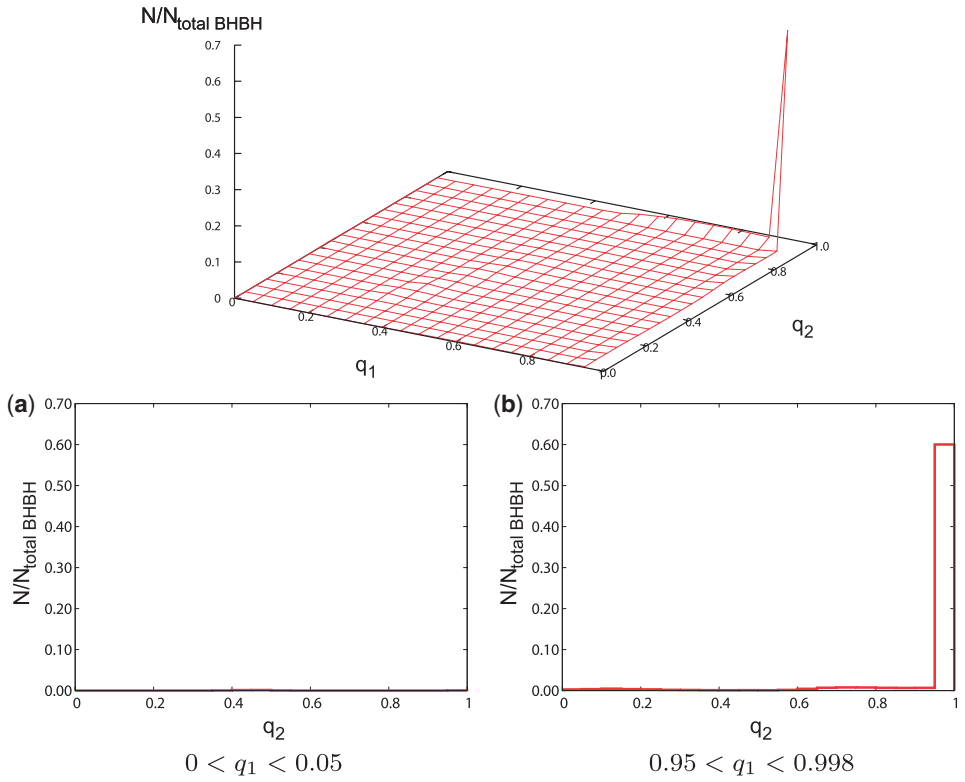

Fig. 11. (Top) The distribution of spin parameters for the $\alpha\lambda = 0.01$ model, with $N_{\rm total\ BHBH} = 27790$. (Bottom) Cross-section views of the distribution of spin parameters for the $\alpha\lambda = 0.01$ model. The format is the same as Fig. 6.

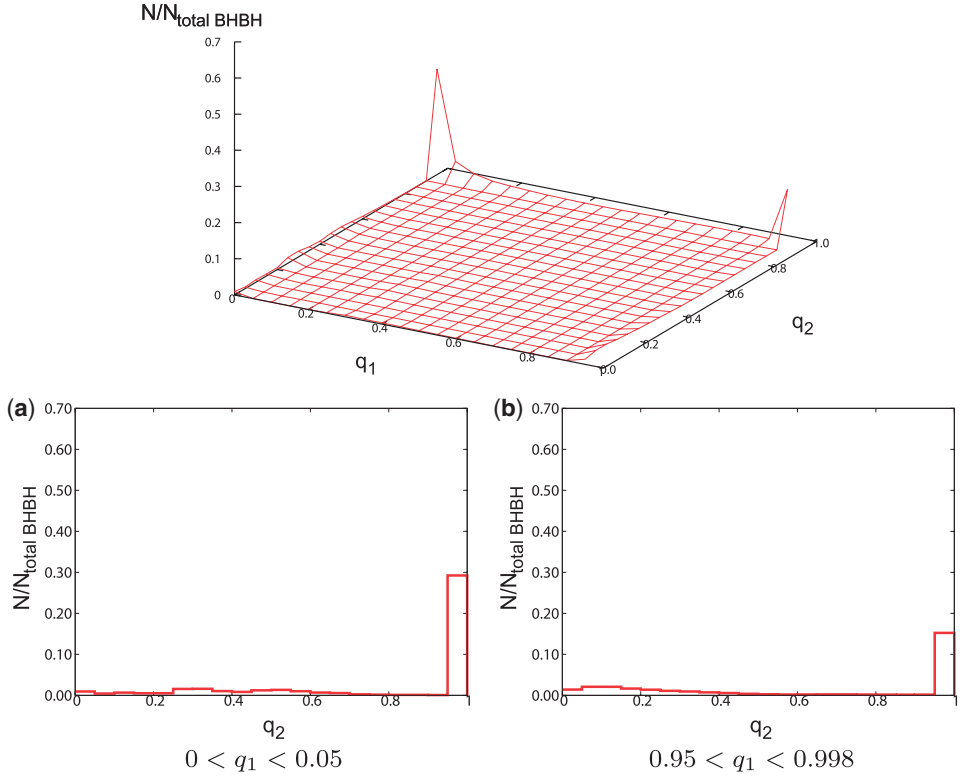

Fig. 12. (Top) The distribution of spin parameters for the $\alpha\lambda = 0.1$ model, with $N_{\rm total\ BHBH} = 124834$. (Bottom) Cross-section views of the distribution of spin parameters for the $\alpha\lambda = 0.1$ model. The format is the same as Fig. 6.

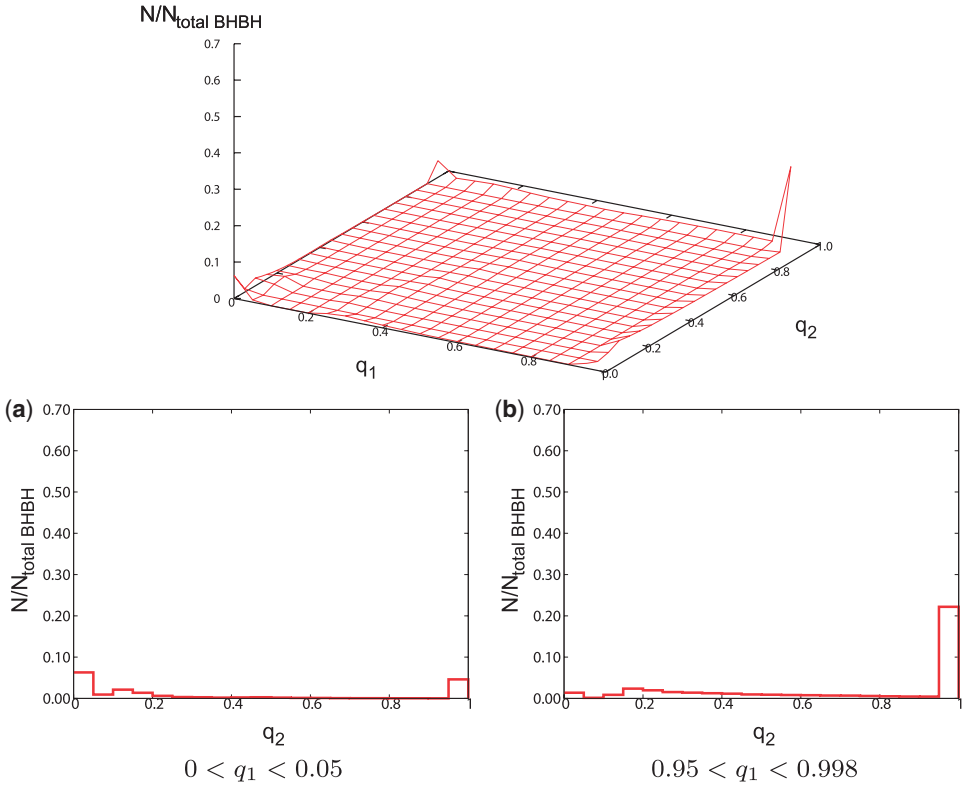

Fig. 13. (Top) The distribution of spin parameters for the $\alpha\lambda = 10$ model, with $N_{\rm total\,BHBH} = 93731$. (Bottom) Cross-section views of the distribution of spin parameters for the $\alpha\lambda = 10$ model. The format is the same as Fig. 6.

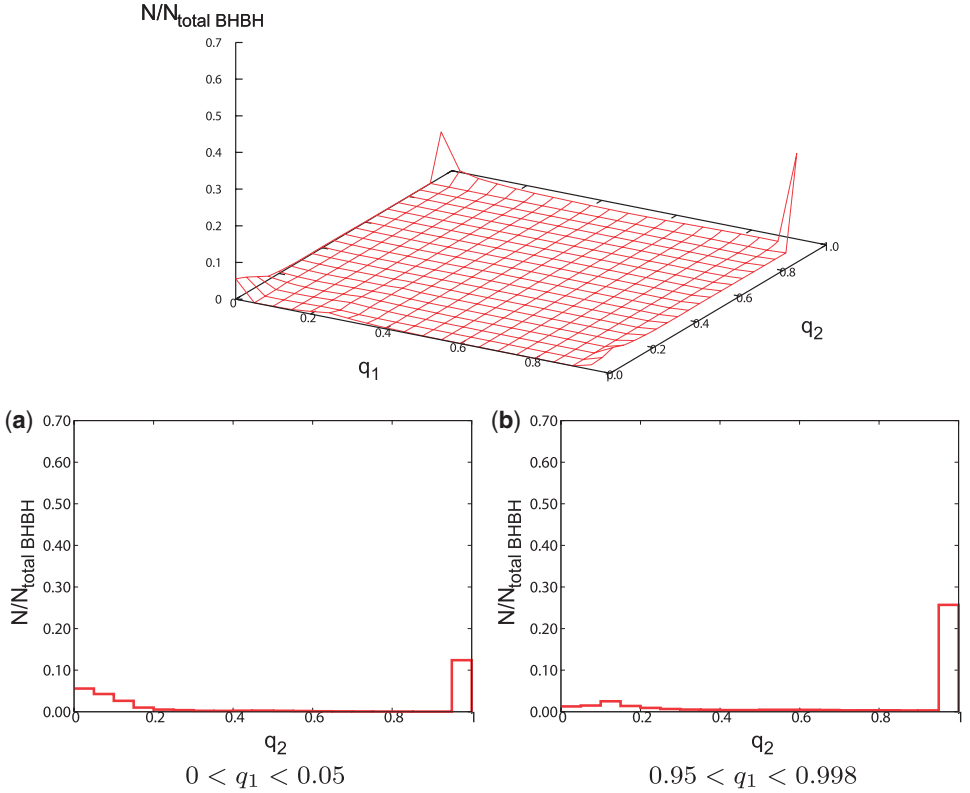

Fig. 14. (Top) The distribution of spin parameters for the $\beta = 0.5$ model, with $N_{\rm total\,BHBH} = 126093$. (Bottom) Cross-section views of the distribution of spin parameters for the $\beta = 0.5$ model. The format is the same as Fig. 6.

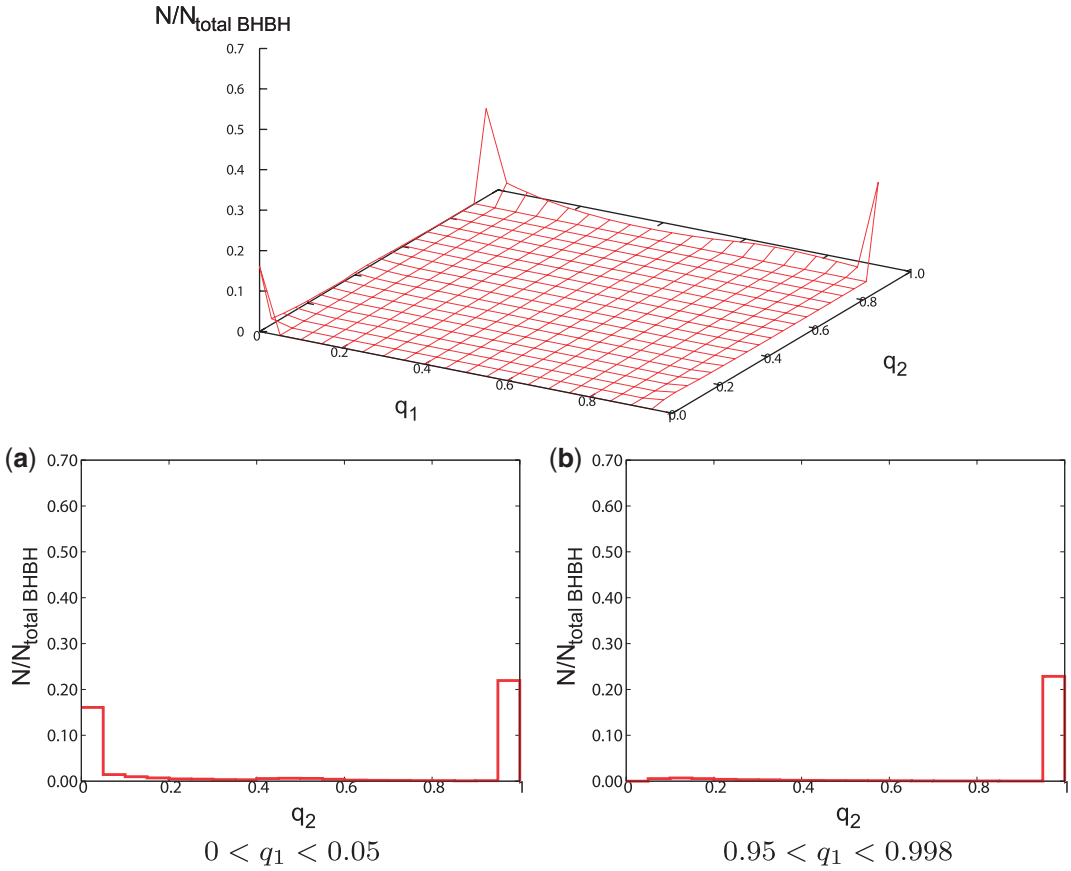

Fig. 15. (Top) The distribution of spin parameters for the $\beta = 1$ model, with $N_{\rm total\,BHBH} = 57028$. (Bottom) Cross-section views of the distribution of spin parameters for the $\beta = 1$ model. The format is the same as Fig, 6.

the CE phase only once do not merge during the CE phase, and the Pop III BBHs which cannot merge within the Hubble time in our standard model come to be able to merge within the Hubble time due to small $\alpha\lambda$. In the $\alpha\lambda = 10$ model, the shape of the spin distribution is almost the same as that of our standard model. The difference in this model from our standard model is the small increase of the fraction of group 2, because the progenitors which merge during the CE phase in our standard model come to be able to survive due to large $\alpha\lambda$.

As for the β dependence (see Figs. 6, 14, and 15), not only the stellar mass loss during RLOF but also the criterion of dynamically unstable mass transfer such as a CE phase are changed by β. In the $\beta = 0.5$ model, the fraction of group 1 is larger than that of our standard model because in this model the progenitors less frequently enter the CE phase than those of our standard model. In the $\beta = 1$ model, the fraction of group 1 is larger than that of our standard model, like a $\beta = 0.5$ model. However, the fraction of group 1 is smaller than that of the $\beta = 0.5$ model because in this model the progenitors lose a lot of angular momentum during the RLOF due to the high β. In this model, since the mass transfer cannot become dynamically unstable, the evolution passes via CE phases as follows. The progenitors of group 2 enter the CE phase when the primary and secondary become giants at the same time, and plunge into each other. On the other hand, the progenitors of group 3 enter the CE phase when the secondary plunges into the primary envelope due to the initial eccentricity.

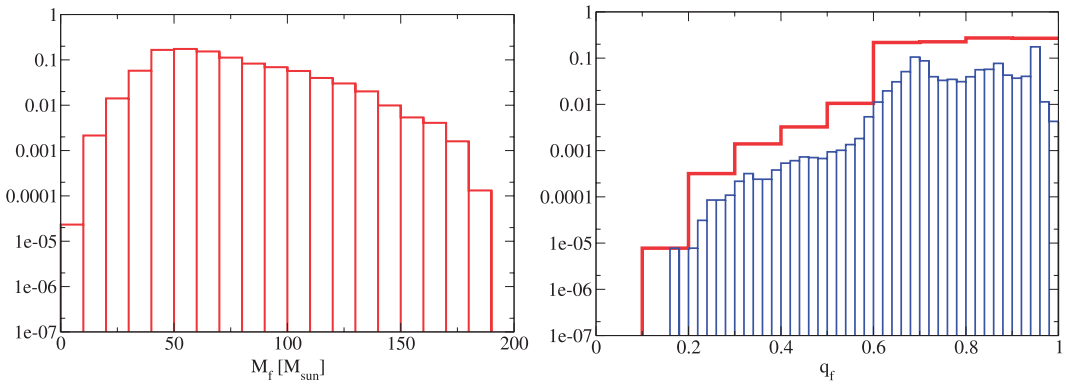

Fig. 16. The remnant mass M_f (left) and spin q_f (right) for our standard model.

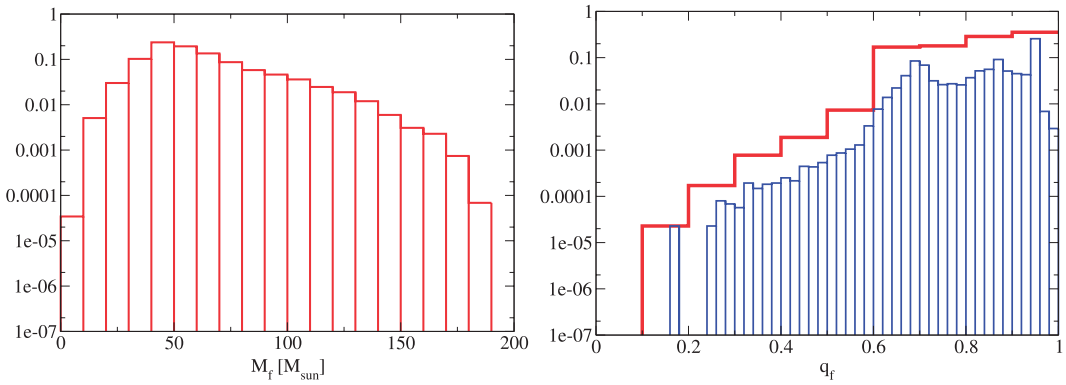

Fig. 17. The remnant mass M_f (left) and spin q_f (right) for the IMF: logflat model.

5. Remnant and event rate for ringdown gravitational waves

5.1. Remnant mass and spin

Based on Ref. [11] (see also Refs. [20,21]), we calculate the remnant mass M_f and spin q_f from given BH binary parameters, M_1, M_2, q_1, and q_2 (see Ref. [4] for a detailed discussion). The remnant mass and spin for each case is shown in Figs. 16–25. Here, we have normalized the distribution, and used binning with $\Delta M_f = 10\,M_\odot$ for M_f and $\Delta q_f = 0.1$ (thick, red) and 0.02 (thin, blue) for q_f.

The IMF dependence shown in Figs. 16, 17, and 18 is described below for the remnant mass and spin. When we treat the steeper IMF, we have a lower number of high-mass remnants. On the other hand, the number of high-spin remnants increases slightly in the steeper IMF cases. This is because in the steeper IMF models we have a large number of progenitors with mass smaller than $50\,M_\odot$.

As for the IEF dependence, we find that in Figs. 16, 19, and 20 there is no strong tendency.

Next, from Figs. 16, 21, 22, and 23 the CE parameter dependence can be described. In the $\alpha\lambda = 0.01$ model, the maximum of the remnant mass becomes much smaller than that of our standard model. This is because the high-mass progenitors merge during a CE phase due to too-small $\alpha\lambda$. As for the remnant spin, we do not have remnant spins which are smaller than 0.55 since BBHs tend to be of equal mass. If a light BH falls into a non-spinning massive BH, the remnant BH can have a small spin ($q_f < 0.6$). However, in the above model many BBHs are equal mass. In the $\alpha\lambda = 0.1$ model, the maximum remnant mass is smaller than that of our standard model again. In this model, the fraction of remnant spins with $0.7 < q_f < 0.8$ is larger than that for our standard model because the fraction of group 3 in this model is larger than in our standard model.

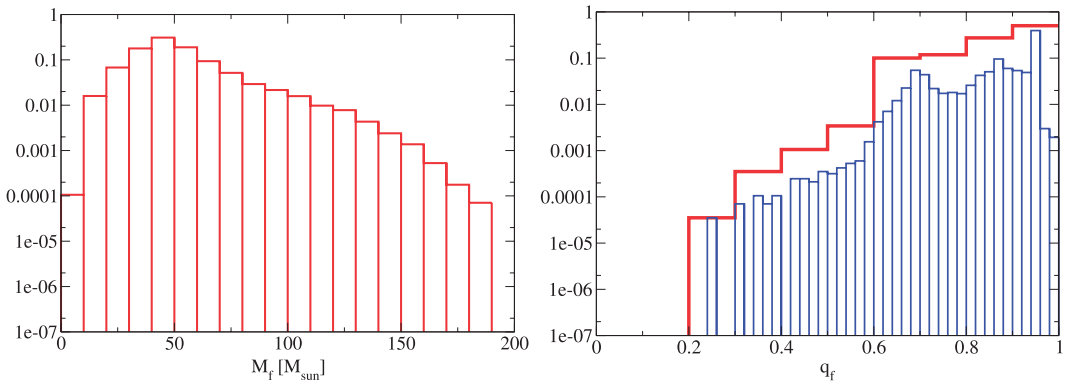

Fig. 18. The remnant mass M_f (left) and spin q_f (right) for the IMF: Salpeter model.

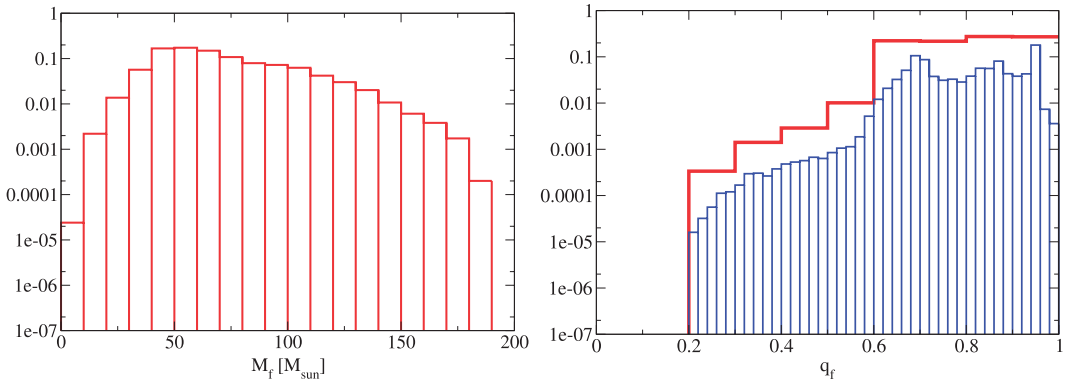

Fig. 19. The remnant mass M_f (left) and spin q_f (right) for the IEF: e =const model.

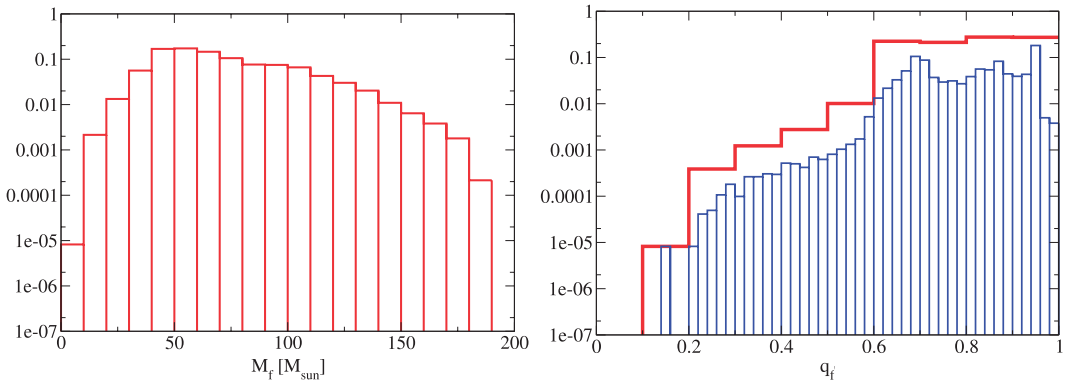

Fig. 20. The remnant mass M_f (left) and spin q_f (right) for the IEF: $e^{-0.5}$ model.

As for the β dependence, we find from Figs. 16, 24, and 25 that the maximum remnant mass becomes lower for higher β, due to the mass loss during RLOF.

5.2. Event rates for ringdown gravitational waves

To estimate the event rate for ringdown gravitational waves, it is necessary to have the merger rate density of Pop III BBHs. The merger rate density R_m [Myr^{-1} Mpc^{-3}] has been derived for various models in Ref. [6], and can be approximated by a fitting formula for low redshift. This is summarized in Table 2. In practice, we have considered the fitting for R_m in terms of redshift z up to $z = 2$, but

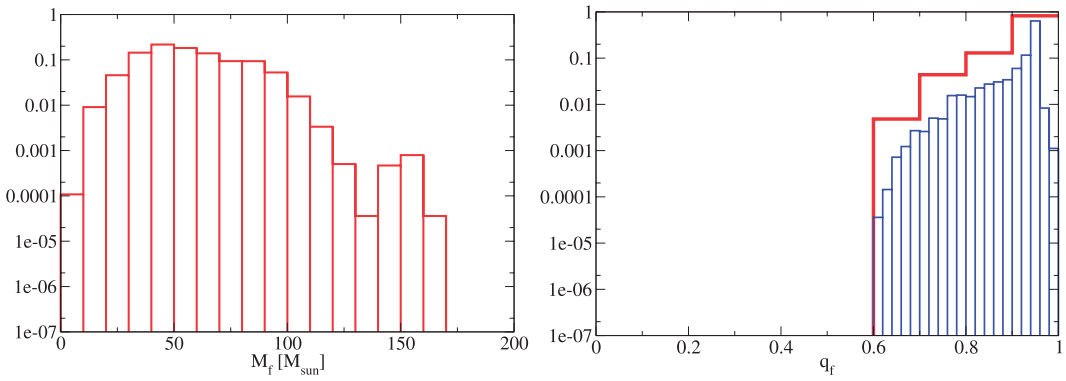

Fig. 21. The remnant mass M_f (left) and spin q_f (right) for the $\alpha\lambda = 0.01$ model.

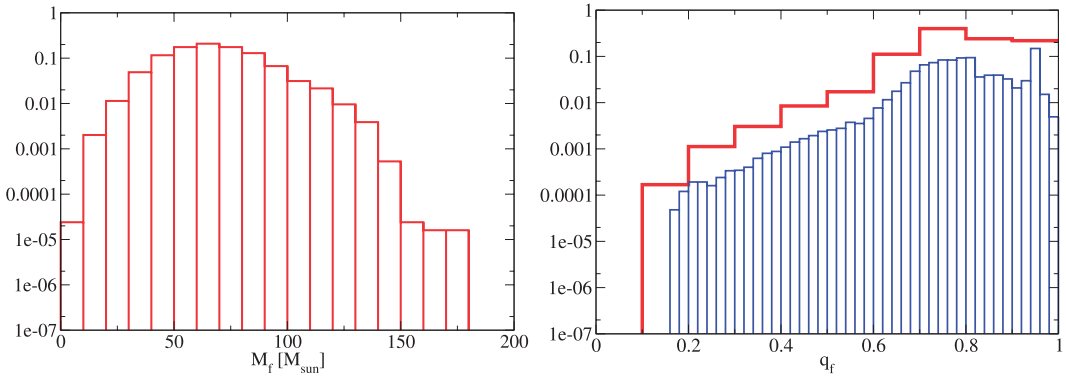

Fig. 22. The remnant mass M_f (left) and spin q_f (right) for the $\alpha\lambda = 0.1$ model.

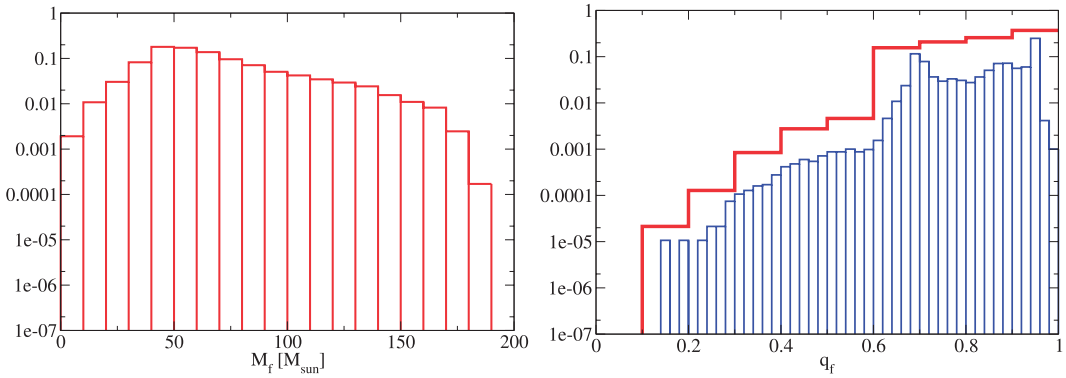

Fig. 23. The remnant mass M_f (left) and spin q_f (right) for the $\alpha\lambda = 10$ model.

the above R_m is derived by using $z \propto D$ where D denotes the (luminosity) distance, because we use it only up to $z \sim 0.2$ in this paper.

Using Ref. [22], we calculate the angle-averaged signal-to-noise ratio (SNR) as

$$\mathrm{SNR} = \sqrt{\frac{8}{5}}\frac{4\eta}{F(q_f)}\sqrt{\frac{\epsilon_r M_f}{S_n(f_c)}}\frac{M_f}{D}, \tag{13}$$

where we assume $\epsilon_r = 3\%$ of the total mass energy radiated in the ringdown phase. Note that for simplicity, any effect of the cosmological distance is ignored here. The symmetric mass ratio

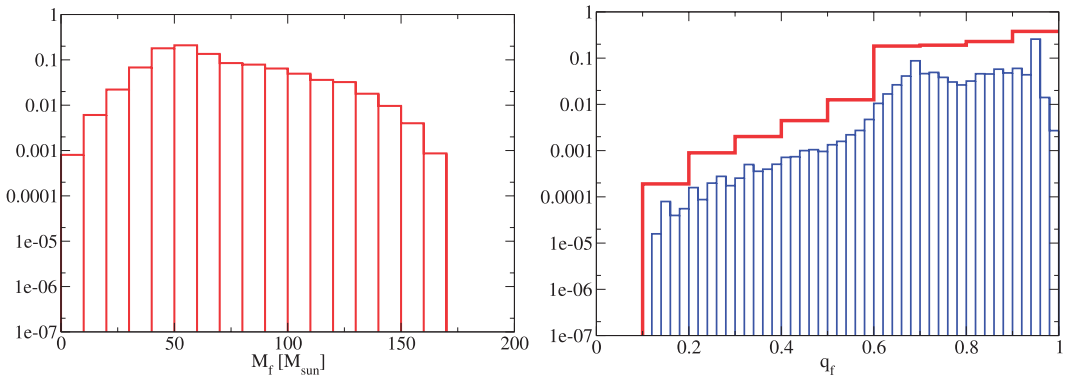

Fig. 24. The remnant mass M_f (left) and spin q_f (right) for the $\beta = 0.5$ model.

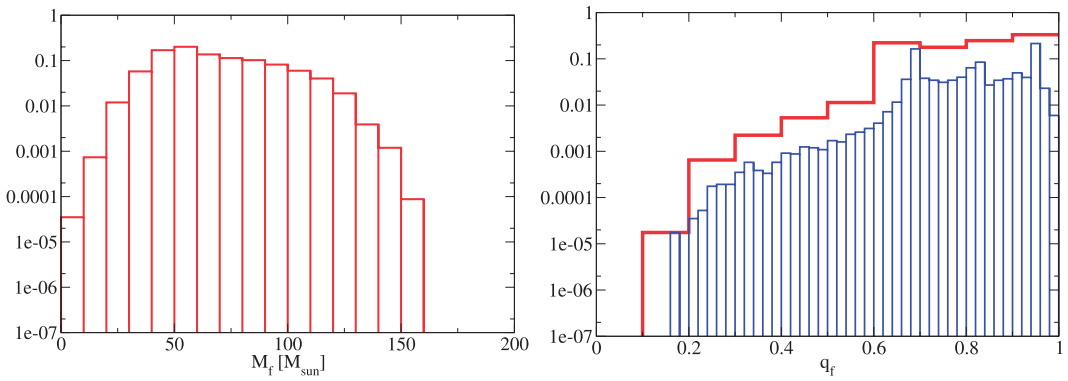

Fig. 25. The remnant mass M_f (left) and spin q_f (right) for the $\beta = 1$ model.

Table 2. Fitting formulas of the merger rate density R_m [Myr^{-1} Mpc^{-3}] for low redshift in the center column. Here, D denotes the (luminosity) distance. In the right column, the event rates [yr^{-1}] divided by dependence on the star formation rate $\mathrm{SFR_p}$ and the fraction of the binary $\mathrm{f_b}$ are shown for each model. We consider events with SNR > 8 for the KAGRA detector here.

Model	R_m [Myr^{-1} Mpc^{-3}]	SNR > 8
Standard	$0.024 + 0.0080\ (D/1\,\mathrm{Gpc})$	446
IMF: logflat	$0.023 + 0.0064\ (D/1\,\mathrm{Gpc})$	255
IMF: Salpeter	$0.014 + 0.0034\ (D/1\,\mathrm{Gpc})$	61.5
IEF: e =const	$0.023 + 0.0075\ (D/1\,\mathrm{Gpc})$	452
IEF: $e^{-0.5}$	$0.022 + 0.0071\ (D/1\,\mathrm{Gpc})$	451
$\alpha\lambda = 0.01$	$0.0024 + 0.0018\ (D/1\,\mathrm{Gpc})$	5.87
$\alpha\lambda = 0.1$	$0.019 + 0.0089\ (D/1\,\mathrm{Gpc})$	146
$\alpha\lambda = 10$	$0.017 + 0.0066\ (D/1\,\mathrm{Gpc})$	372
$\beta = 0.5$	$0.030 + 0.0099\ (D/1\,\mathrm{Gpc})$	499
$\beta = 1$	$0.017 + 0.0029\ (D/1\,\mathrm{Gpc})$	158

$\eta = M_1 M_2/(M_1 + M_2)^2$ is evaluated from the inspiral phase, and

$$F(q_f) = 1.5251 - 1.1568(1 - q_f)^{0.1292}, \quad f_c = \frac{1}{2\pi M_f} F(q_f) \tag{14}$$

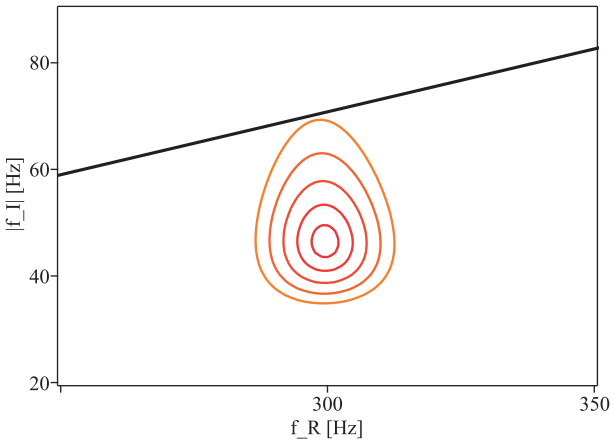

Fig. 26. In the (f_R, f_I) plane, we show the parameter estimation in a case with SNR $= 35$ for the typical case [5,6] (with $M_{\rm rem} = 57.0904\,M_\odot$ and $\alpha_{\rm rem} = 0.686710$). The (black) thick line shows the Schwarzschild limit and the ellipses are the contours of $1\,\sigma$, $2\,\sigma$, $3\,\sigma$, $4\,\sigma$, and $5\,\sigma$. In general relativity, the top-left side of the thick black line is prohibited.

are obtained from the remnant BH's mass and spin (see Ref. [23]). We evaluate the above SNR of the QNM GWs in the expected KAGRA noise curve $S_n(f)$ [9,10] [bKAGRA, VRSE(D) configuration] (see Ref. [4] for the detailed calculation). This noise curve is presented in Ref. [26], and we use the fitting noise curve obtained in Ref. [24], based on Ref. [26]. Then, the event rate for a given SNR is derived by using the merger rate density in Table 2. In the right column of Table 2, we present the event rate with SNR > 8. Here, the event rates [yr^{-1}] have been divided by dependence on the star formation rate $\mathrm{SFR_p}$ and the fraction of the binary $\mathrm{f_b}$.

In Fig. 26, based on Ref. [24], we show the parameter estimation in a case with SNR $= 35$ for the typical case [5,6] (with $M_{\rm rem} = 57.0904\,M_\odot$ and $\alpha_{\rm rem} = 0.686710$). The (black) thick line shows the Schwarzschild limit and the ellipses are the contours of $1\,\sigma$, $2\,\sigma$, $3\,\sigma$, $4\,\sigma$, and $5\,\sigma$. In general relativity, the top-left side of the thick black line is prohibited. Thus, using the event with SNR > 35, we summarize various event rates in Tables 3 and 4. Table 3 shows the total event rates [yr^{-1}] divided by dependence on the star formation rate $\mathrm{SFR_p}$ and the fraction of the binary $\mathrm{f_b}$ for ten models, and those for a remnant BH with $q_f > 0.7$, 0.9, and 0.95.

In Table 4, we present the detection rate [yr^{-1}] divided by dependence on the star formation rate $\mathrm{SFR_p}$ and the fraction of the binary $\mathrm{f_b}$ as a function of the lower limit of the solid angle of a sphere $4\pi C$ by which we can estimate the contribution of the ergoregion. The relation between this C and the spin parameter q was obtained in Ref. [27] (see also the recent studies in [25,27–29]). It is noted that $q_f > 0.9$ corresponds to $C \gtrsim 0.97$.

6. Discussions

In this paper, we extended our previous work [4] (the standard model in this paper) by looking at the dependence on various parameters of the Pop III binary population synthesis calculation. As shown in the right column of Table 2, the detection rate with SNR > 8 for the second-generation GW detectors such as KAGRA was obtained as 5.9–500 events yr^{-1} $(\mathrm{SFR_p}/(10^{-2.5}\,M_\odot\,\mathrm{yr}^{-1}\,\mathrm{Mpc}^{-3}))\cdot([\mathrm{f_b}/(1+\mathrm{f_b})]/0.33)$ between ten models. Recently, Kushnir et al. [30] have discussed whether the BH's spin constrains the binary evolution path in the case of Pop I and Pop II binaries. If we detect a lot of Pop III BBH mergers, we might be able to constrain the Pop III binary evolution paths not only

Table 3. The total event rate [yr^{-1}] divided by dependence on the star formation rate $\mathrm{SFR_p}$ and the fraction of the binary $\mathrm{f_b}$ for each model and those for the final $q_f > 0.7$, 0.9, and 0.95 BHs in the case of SNR > 35 for the KAGRA detector.

Model	all	$0.7 < q_f$	$0.9 < q_f$	$0.95 < q_f$
Standard	3.73	2.45	0.115	0.0260
IMF: logflat	2.17	1.41	0.0659	0.0152
IMF: Salpeter	0.530	0.337	0.0153	0.00300
IEF: $e = $ const.	3.80	2.38	0.0943	0.0248
IEF: $e^{-0.5}$	3.82	2.38	0.0800	0.0228
$\alpha\lambda = 0.01$	0.0463	0.0411	0.00832	0.00268
$\alpha\lambda = 0.1$	1.23	0.864	0.0377	0.0114
$\alpha\lambda = 10$	2.96	2.16	0.243	0.0372
$\beta = 0.5$	4.21	3.29	0.0981	0.0157
$\beta = 1$	1.58	0.705	0.0185	0.0128

Table 4. The event rates [yr^{-1}] divided by dependence on the star formation rate $\mathrm{SFR_p}$ and the fraction of the binary $\mathrm{f_b}$ as a function of the lower limit of the solid angle of a sphere $4\pi C$, where the QNM is mainly emitted from the ergoregion, in the case of SNR > 35 for the KAGRA detector.

Model	$0.5 < C$	$0.7 < C$	$0.9 < C$	$0.95 < C$	$0.97 < C$	$0.99 < C$
Standard	2.23	1.10	0.356	0.162	0.117	0.0780
IMF: logflat	1.29	0.621	0.207	0.102	0.0683	0.0454
IMF: Salpeter	0.309	0.145	0.0489	0.0234	0.0156	0.00960
IEF: $e = $ const.	2.18	0.998	0.288	0.132	0.0955	0.0621
IEF: $e^{-0.5}$	2.15	0.936	0.237	0.115	0.0825	0.0518
$\alpha\lambda = 0.01$	0.0399	0.0318	0.0131	0.00966	0.00839	0.00503
$\alpha\lambda = 0.1$	0.820	0.391	0.135	0.0609	0.0390	0.0222
$\alpha\lambda = 10$	2.01	1.09	0.470	0.307	0.246	0.187
$\beta = 0.5$	3.09	0.979	0.294	0.127	0.0990	0.0292
$\beta = 1$	0.666	0.405	0.0278	0.0218	0.0187	0.0141

by the mass distribution but also by the spin distribution. In particular, as described in Sect. 4, the spin of a black hole depends strongly on whether the progenitor of black hole enters the CE phase or not. Thus, we can check whether a BBH progenitor evolved via the CE phase or not by the spins of the BBH.

One of the interesting outputs from the QNM GWs is whether we can confirm the ergoregion of the Kerr BH. From Table 4, the event rate for the confirmation of $> 50\%$ of the ergoregion is 0.040–3.1 events yr^{-1} $(\mathrm{SFR_p}/(10^{-2.5}\,M_\odot\,\mathrm{yr}^{-1}\,\mathrm{Mpc}^{-3})) \cdot ([\mathrm{f_b}/(1+\mathrm{f_b})]/0.33)$ with SNR > 35.

When we consider extracting the rotational energy of BHs using the Penrose process [31] or the Blanford–Znajek process [32], for example, we want to observe highly spinning remnant BHs. For remnant BHs with spin $q_f > 0.95$, the event rate with SNR > 35 is 0.0027–0.037 events yr^{-1} $(\mathrm{SFR_p}/(10^{-2.5}\,M_\odot\,\mathrm{yr}^{-1}\,\mathrm{Mpc}^{-3})) \cdot ([\mathrm{f_b}/(1+\mathrm{f_b})]/0.33)$ in the KAGRA detector from Table 3. A third-generation GW observatory, the Einstein Telescope [33] will have an improvement in sensitivity of about a factor of ten over second-generation detectors. This means that we have roughly 1000 times higher expected event rates, and, for example, the ringdown event rate with

$q_f > 0.95$ will become

$$3\text{–}30\ \text{events}\ \text{yr}^{-1} \left(\frac{\text{SFR}_\text{p}}{10^{-2.5}\ \text{M}_\odot\ \text{yr}^{-1}\ \text{Mpc}^{-3}}\right) \cdot \left(\frac{\text{f}_\text{b}/(1+\text{f}_\text{b})}{0.33}\right) \left(\frac{\epsilon_r}{0.03}\right)^{1/2}. \quad (15)$$

Here, we have introduced ϵ_r as the fraction of the BH mass radiated in the ringdown phase, and assumed $\epsilon_r = 3\%$ to calculate the SNR and the event rates in this paper. If $\epsilon_r = 0.3\%$, we will still have the possibility of detecting QNM GWs from highly spinning remnant BHs.

Finally, Pop III BBH mergers can be a target for space-based GW detectors such as eLISA [34] and DECIGO [35]. Study in this direction is one of our future works.

Acknowledgements

This work was supported by MEXT Grant-in-Aid for Scientific Research on Innovative Areas, "New Developments in Astrophysics Through Multi-Messenger Observations of Gravitational Wave Sources," Nos. 24103001 and 24103006 (HN, TN), JSPS Grant-in-Aid for Scientific Research (C), No. 16K05347 (HN), and Grant-in-Aid from the Ministry of Education, Culture, Sports, Science, and Technology (MEXT) of Japan No. 15H02087 (TN).

References

[1] V. Cardoso, E. Franzin, and P. Pani, Phys. Rev. Lett. **116**, 171101 (2016) [arXiv:1602.07309 [gr-qc]] [Search INSPIRE].
[2] R. P. Kerr, Phys. Rev. Lett. **11**, 237 (1963).
[3] E. Berti et al., Class. Quant. Grav. **32**, 243001 (2015) [arXiv:1501.07274 [gr-qc]] [Search INSPIRE].
[4] T. Kinugawa, H. Nakano, and T. Nakamura, Prog. Theor. Exp. Phys. **2016**, 031E01 (2016) [arXiv:1601.07217 [astro-ph.HE]] [Search INSPIRE].
[5] T. Kinugawa, K. Inayoshi, K. Hotokezaka, D. Nakauchi, and T. Nakamura, Mon. Not. Roy. Astron. Soc. **442**, 2963 (2014) [arXiv:1402.6672 [astro-ph.HE]] [Search INSPIRE].
[6] T. Kinugawa, A. Miyamoto, N. Kanda, and T. Nakamura, Mon. Not. Roy. Astron. Soc. **456**, 1093 (2016) [arXiv:1505.06962 [astro-ph.SR]] [Search INSPIRE].
[7] J. Aasi et al. [LIGO Scientific Collaboration], Class. Quant. Grav. **32**, 074001 (2015) [arXiv:1411.4547 [gr-qc]] [Search INSPIRE].
[8] F. Acernese et al. [VIRGO Collaboration], Class. Quant. Grav. **32**, 024001 (2015) [arXiv:1408.3978 [gr-qc]] [Search INSPIRE].
[9] K. Somiya [KAGRA Collaboration], Class. Quant. Grav. **29**, 124007 (2012) [arXiv:1111.7185 [gr-qc]] [Search INSPIRE].
[10] Y. Aso et al. [KAGRA Collaboration], Phys. Rev. D **88**, 043007 (2013) [arXiv:1306.6747 [gr-qc]] [Search INSPIRE].
[11] J. Healy, C. O. Lousto, and Y. Zlochower, Phys. Rev. D **90**, 104004 (2014) [arXiv:1406.7295 [gr-qc]] [Search INSPIRE].
[12] J. R. Hurley, C. A. Tout, and O. R. Pols, Mon. Not. Roy. Astron. Soc. **329**, 897 (2002) [arXiv:astro-ph/0201220] [Search INSPIRE].
[13] S. Hirano, T. Hosokawa, N. Yoshida, H. Umeda, K. Omukai, G. Chiaki, and H. W. Yorke, Astrophys. J. **781**, 60 (2014) [arXiv:1308.4456 [astro-ph.CO]] [Search INSPIRE].
[14] H. Susa, K. Hasegawa, and N. Tominaga, Astrophys. J. **792**, 32 (2014) [arXiv:1407.1374 [astro-ph.GA]] [Search INSPIRE].
[15] P. Eggleton, *Evolutionary Processes in Binary and Multiple Stars* (Cambridge University Press, Cambridge, UK, 2011)
[16] R. F. Webbink, Astrophys. J. **277**, 355 (1984).
[17] P. Marigo, L. Girardi, C. Chiosi, and P. R. Wood, Astron. Astrophys. **371**, 152 (2001) [arXiv:astro-ph/0102253] [Search INSPIRE].
[18] K. S. Thorne, Astrophys. J. **191**, 507 (1974).
[19] N. Ivanova et al., Astron. Astrophys. Rev. **21**, 59 (2013) [arXiv:1209.4302 [astro-ph.HE]] [Search INSPIRE].

[20] E. Barausse, V. Morozova, and L. Rezzolla, Astrophys. J. **758**, 63 (2012); **786**, 76 (2014) [erratum] [arXiv:1206.3803 [gr-qc]] [Search INSPIRE].
[21] F. Hofmann, E. Barausse, and L. Rezzolla, arXiv:1605.01938 [gr-qc] [Search INSPIRE].
[22] E. E. Flanagan and S. A. Hughes, Phys. Rev. D **57**, 4535 (1998) [arXiv:gr-qc/9701039] [Search INSPIRE].
[23] E. Berti, V. Cardoso, and C. M. Will, Phys. Rev. D **73**, 064030 (2006) [arXiv:gr-qc/0512160] [Search INSPIRE].
[24] H. Nakano, T. Tanaka, and T. Nakamura, Phys. Rev. D **92**, 064003 (2015) [arXiv:1506.00560 [astro-ph.HE]] [Search INSPIRE].
[25] T. Nakamura, H. Nakano, and T. Tanaka, Phys. Rev. D **93**, 044048 (2016) [arXiv:1601.00356 [astro-ph.HE]] [Search INSPIRE].
[26] ICRR GW Group, *KAGRA official sensitivity limit* (ICRR GW Group, Tokyo, 2010). (Available at: http://gwcenter.icrr.u-tokyo.ac.jp/researcher/parameters, date last accessed September 14, 2016).
[27] H. Nakano, T. Nakamura, and T. Tanaka, Prog. Theor. Exp. Phys. **2016**, 031E02 (2016) [arXiv:1602.02875 [gr-qc]] [Search INSPIRE].
[28] T. Nakamura and H. Nakano, Prog. Theor. Exp. Phys. **2016**, 041E01 (2016) [arXiv:1602.02385 [gr-qc]] [Search INSPIRE].
[29] H. Nakano, N. Sago, T. Tanaka, and T. Nakamura, arXiv:1604.08285 [gr-qc] [Search INSPIRE].
[30] D. Kushnir, M. Zaldarriaga, J. A. Kollmeier, and R. Waldman, arXiv:1605.03839 [astro-ph.HE] [Search INSPIRE].
[31] R. Penrose, Riv. Nuovo Cim. **1**, 252 (1969) [Gen. Rel. Grav. **34**, 1141 (2002)].
[32] R. D. Blandford and R. L. Znajek, Mon. Not. Roy. Astron. Soc. **179**, 433 (1977).
[33] M. Punturo et al., Class. Quant. Grav. **27**, 194002 (2010).
[34] P. A. Seoane et al. [eLISA Collaboration], arXiv:1305.5720 [astro-ph.CO] [Search INSPIRE].
[35] N. Seto, S. Kawamura, and T. Nakamura, Phys. Rev. Lett. **87**, 221103 (2001) [arXiv:astro-ph/0108011] [Search INSPIRE].